Cell Metabolism
Article

DNA Damage Triggers a Chronic Autoinflammatory Response, Leading to Fat Depletion in NER Progeria

Ismene Karakasilioti,[1,3] Irene Kamileri,[1,3] Georgia Chatzinikolaou,[1] Theodoros Kosteas,[1] Eleni Vergadi,[5] Andria Rasile Robinson,[6] Iannis Tsamardinos,[2,4] Tania A. Rozgaja,[7] Sandra Siakouli,[3] Christos Tsatsanis,[5] Laura J. Niedernhofer,[6,7,8] and George A. Garinis[1,3,*]

[1]Institute of Molecular Biology and Biotechnology
[2]Bioinformatics Laboratory, Institute of Computer Science
Foundation for Research and Technology-Hellas, 70013 Heraklion, Crete, Greece
[3]Department of Biology
[4]Department of Computer Sciences
University of Crete, 71409 Heraklion, Crete, Greece
[5]Department of Clinical Chemistry, School of Medicine, University of Crete, 71003 Heraklion, Crete, Greece
[6]University of Pittsburgh Cancer Institute, Pittsburgh, PA 15232, USA
[7]Department of Metabolism & Aging, The Scripps Research Institute, Florida, 130 Scripps Way, 3B3, Jupiter, FL 33458, USA
[8]Department of Microbiology and Molecular Genetics, University of Pittsburgh School of Medicine, Pittsburgh, PA 15219, USA
*Correspondence: garinis@imbb.forth.gr
http://dx.doi.org/10.1016/j.cmet.2013.08.011

SUMMARY

Lipodystrophies represent a group of heterogeneous disorders characterized by loss of fat tissue. However, the underlying mechanisms remain poorly understood. Using mice carrying an ERCC1-XPF DNA repair defect systematically or in adipocytes, we show that DNA damage signaling triggers a chronic autoinflammatory response leading to fat depletion. *Ercc1*$^{-/-}$ and aP2-*Ercc1*$^{F/-}$ fat depots show extensive gene expression similarities to lipodystrophic *Pparγ*$^{ldi/+}$ animals, focal areas of ruptured basement membrane, the reappearance of primary cilia, necrosis, fibrosis, and a marked decrease in adiposity. We find that persistent DNA damage in aP2-*Ercc1*$^{F/-}$ fat depots and in adipocytes ex vivo triggers the induction of proinflammatory factors by promoting transcriptionally active histone marks and the dissociation of nuclear receptor corepressor complexes from promoters; the response is cell autonomous and requires ataxia telangiectasia mutated (ATM). Thus, persistent DNA damage-driven autoinflammation plays a causative role in adipose tissue degeneration, with important ramifications for progressive lipodystrophies and natural aging.

INTRODUCTION

In humans, the causative role of DNA damage in age-related diseases is supported by several premature aging-like (progeroid) disorders with defects in DNA repair (Kamileri et al., 2012a; Schumacher et al., 2009). Nucleotide excision repair (NER) represents one such pathway that operates via a "cut and patch" mechanism and proceeds in successive steps, beginning with lesion recognition, unwinding of the double helix at damaged DNA sites, and lesion verification, followed by excision of the DNA damage and gap-filling DNA synthesis (Kamileri et al., 2012a). NER is divided into two subpathways, global genome repair (GGR) and transcription-coupled repair (TCR), differing primarily in how the damage is initially recognized (Hanawalt, 2002). In humans, defects in GGR cause the cancer-prone syndrome xeroderma pigmentosum (XP, complementation groups XP-A to XP-G) (DiGiovanna and Kraemer, 2012). Conversely, defects in TCR give rise to a heterogeneous group of progeroid syndromes, including the Cockayne syndrome (CS), trichothiodystrophy (TTD), or XFE (Kamileri et al., 2012a). CS, TTD, and XFE patients are characterized by postnatal growth failure, skeletal and neuronal abnormalities, depletion of subcutaneous fat depots, and short lifespan, but not cancer (Garinis et al., 2008; Kamileri et al., 2012a).

Whereas genome instability has been established as the underlying cause of mutations leading to increased skin cancer predisposition in XP, the functional links between defective NER and the manifestation of progeroid or developmental defects remain obscure (Kamileri et al., 2012a). Using ERCC1-defective animal models of a human progeroid syndrome (Niedernhofer et al., 2006), we provide evidence for a causal link between persistent DNA damage and the gradual manifestation of progressive lipodystrophy in NER progerias; we find that the accumulation of irreparable DNA interstrand crosslinks (ICLs) triggers the transcriptional derepression of proinflammatory cytokines in adipocytes, the recruitment of leukocytes to sites of tissue damage, and the destruction of white adipose tissue depots in NER-defective animals. Taken together, our findings provide a mechanism by which stochastic, endogenous DNA damage instigates tissue-specific pathology in progeroid syndromes and, by analogy, likely with aging.

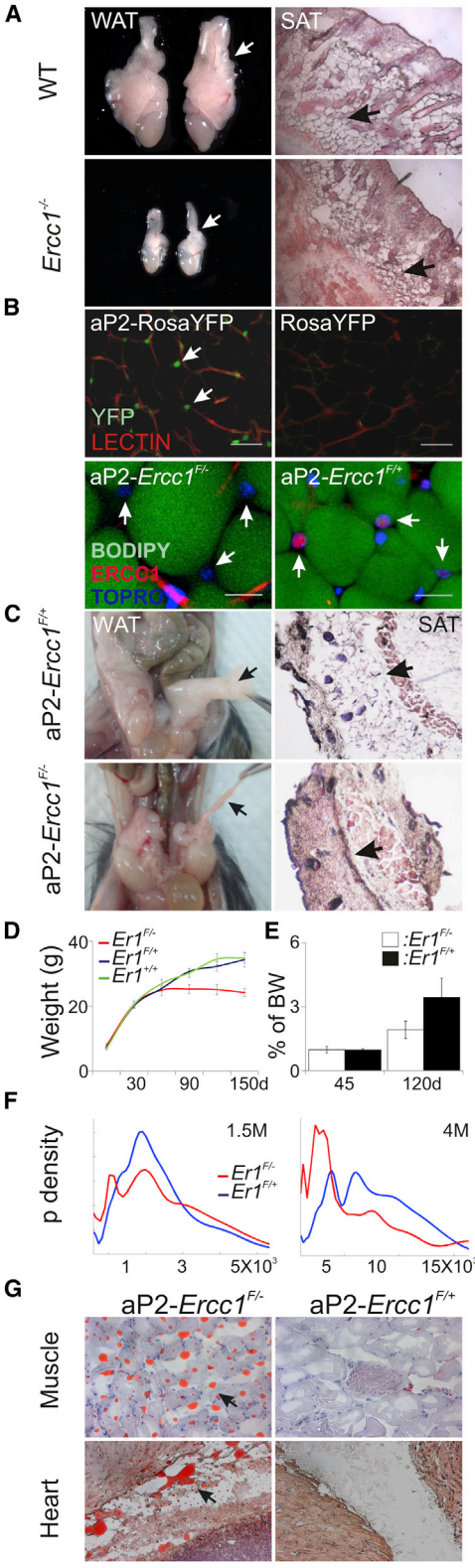

Figure 1. Loss of Fat Depots in *Ercc1*$^{-/-}$ and aP2-*Ercc1*$^{F/-}$ Animals

(A) Photograph of 15-day-old WT and *Ercc1*$^{-/-}$ epididymal white adipose tissue (WAT; embedded arrowheads) and subcutaneous adipose tissue (SAT; embedded arrowheads) depots.

(B) aP2-*Cre*-driven Rosa YFP expression in adipocytes (upper panel) and ERCC1 protein staining indicating cell-type-specific ablation of ERCC1 in aP2-*Ercc1*$^{F/-}$ adipocytes (lower panel), indicated by the respective arrows.

(C) Photograph of 4-month-old aP2-*Ercc1*$^{F/+}$ and aP2-*Ercc1*$^{F/-}$ WAT and SAT depots indicated by the respective arrows.

(D) Weight of aP2-*Ercc1*$^{F/-}$ (*Er1*$^{F/-}$), aP2-*Ercc1*$^{F/+}$ (*Er1*$^{F/+}$), and WT (*Er*$^{+/+}$) animals at the indicated time points.

(E) Weight of WAT depots shown as the percent of body weight (BW).

(F) Size distribution of adipocytes derived from 1.5- and 4-month-old aP2-*Ercc1*$^{F/-}$ (*Er1*$^{F/-}$) and aP2-*Ercc1*$^{F/+}$ (*Er1*$^{F/+}$) animals.

(G) Oil red O staining indicating the accumulation of triglycerides in muscle and heart tissues derived from 4-month-old aP2-*Ercc1*$^{F/-}$ as compared to aP2-*Ercc1*$^{F/+}$ animals (20× magnification). Scale bars: 50 μm (RosaYFP), 20 μm (ERCC1); error bars indicate SEM ($n \geq 3$). See also Figure S1.

RESULTS

Loss of Adipose Tissue in aP2-*Cre* *Ercc1*$^{-/-}$ Animals

Besides dwarfism, CS, TTD, and XFE patients are characterized by loss of subcutaneous fat, which is also seen with normal aging (Sepe et al., 2011). To gain a greater understanding of the role of unrepaired DNA damage in adipose tissue degeneration, we compared the white (WAT) and brown (BAT) adipose fat depots from *Ercc1*$^{-/-}$ mice and animals in which *Ercc1* is knocked out in the fat, causing impaired DNA repair systemically or in adipose tissue, respectively. Beginning at postnatal day 5 (P5), *Ercc1*$^{-/-}$ animals fail to gain weight and display gradual reduction in epididymal, cervical, interscapular, and subcutaneous WAT depots. P15 *Ercc1*$^{-/-}$ mice show an ~50% decrease in epididymal WAT, with most P20 *Ercc1*$^{-/-}$ mice having few or no residual WAT depots with a small (albeit not significant) reduction of BAT depots (Figure 1A; Figures S1A and S1B available online). *Ercc1*$^{-/-}$ mice are growth defective, show premature aging features in several organs, and die of liver failure within a month after birth (Niedernhofer et al., 2006; Selfridge et al., 2001). To test whether fat depletion in *Ercc1*$^{-/-}$ mice is the consequence of defects in other tissues or is cell autonomous, we intercrossed animals homozygous for the floxed *Ercc1* allele (*Ercc1*$^{F/F}$) (Verhagen-Oldenampsen et al., 2012) with those carrying the adipose protein 2 (aP2)-*Cre* transgene in an *Ercc1* heterozygous background; aP2 is a carrier protein for fatty acids that is primarily expressed in adipocytes (Jones et al., 2005). Crossing the aP2 with Rosa YFP transgenic animals confirmed the specificity of aP2-driven YFP expression to adipocytes at P30 (Figure 1B; upper panel), but not at P15 (Figure S1O), the cell type-specific ablation of *Ercc1* in 1.5-month-old aP2-*Ercc1*$^{F/-}$ WAT depots (Figures 1B, lower panel, and S1I), and the normative ERCC1 expression levels in aP2-*Ercc1*$^{F/-}$ organs other than the adipose tissue (Figures S1C, S1K, and S1L). Excision of the floxed *Ercc1* allele was further confirmed by genomic PCR amplification on DNA derived from aP2-*Ercc1*$^{F/+}$ and aP2-*Ercc1*$^{F/-}$ adipose tissues (Figures S1F and S1G) as well as the significant decrease in the *Ercc1* messenger RNA (mRNA) levels in 45-day-old aP2-*Ercc1*$^{F/-}$ adipose WAT depots (Figure S1H). aP2-*Ercc1*$^{F/-}$ mice were born at the expected Mendelian frequency and showed no developmental defects or other pathological features, including any visible defects in adipose tissue; the mRNA levels of *Fabp4* and *Adiponectin*, an adipocyte secretory adipokine previously linked to insulin resistance and diabetes (Kadowaki et al., 2006), were comparable between

1.5-month-old aP2-*Ercc1*$^{F/-}$ WAT tissues and control animals (Figure S1J). Beginning at 2.5 months, aP2-*Ercc1*$^{F/-}$ animals show a slow but steady loss of epididymal, interscapular, and subcutaneous fat depots (Figures 1C and S1D), resulting in an ~30% reduction in body weight (Figure 1D), a >50% reduction in epididymis WAT (Figure 1E), and interscapular BAT depots (Figure S1N); the weight of other organs was comparable to that of control animals (Figure S1E). Unlike the 1.5-month-old aP2-*Ercc1*$^{F/-}$ animals, computer image analysis revealed substantial differences in the number and size of adipocytes of 4-month-old aP2-*Ercc1*$^{F/-}$ animals compared to age-matched controls (Figure 1F). Thus, adult mice lacking ERCC1 specifically in the adipose tissue exhibit marked WAT and BAT abnormalities; importantly, both adipose tissue depots develop normally in these mice, with defects gradually appearing at later stages in life.

Morphological Changes in *Ercc1*$^{-/-}$ and aP2-*Ercc1*$^{F/-}$ Adipose Tissue Depots and aP2-*Ercc1*$^{F/-}$ Metabolic Abnormalities

Oil red O staining of 4-month-old aP2-*Ercc1*$^{F/-}$ tissues revealed accumulation of triglycerides in heart and muscle (Figure 1G), but not in liver, kidney, or spleen (Figure S2A). The 4-month-old aP2-*Ercc1*$^{F/-}$ had normal serum cholesterol levels, a significant increase in triglycerides not seen in 1.5-month-old mice (Figures S2B and S2C), and decreased adiponectin protein levels both in serum and WAT as compared to aP2-*Ercc1*$^{F/+}$ control mice (Figures 2A and S2C). Prior to the glucose and insulin tolerance tests, 4-month-old aP2-*Ercc1*$^{F/-}$ animals had basal plasma glucose levels comparable to wild-type mice after a 5 hr fast (Figures 2B and S2D). Upon intraperitoneal glucose infusion, the 4-month-old, but not the 1.5-month-old, aP2-*Ercc1*$^{F/-}$ mice had increased plasma glucose levels compared to those of controls (Figures 2B and S2E). Staining of pancreata from fasted aP2-*Ercc1*$^{F/-}$ mice and measurement of serum insulin levels revealed an increased number and size of insulin foci and hyperinsulinemia, respectively, compared to aP2-*Ercc1*$^{F/+}$ controls (Figures 2C, 2D, S2F, and S2G). aP2-*Ercc1*$^{F/-}$ and aP2-*Ercc1*$^{F/+}$ animals had comparable serum glucose levels following intraperitoneal insulin infusion (Figure S2D). Food and water intake measurements in 2.5-month-old aP2-*Ercc1*$^{F/-}$ and aP2-*Ercc1*$^{F/+}$ animals over a period of 30 days revealed no significant differences (Figure S2H). Thus, similar to other lipodystrophic animal models, the aP2-*Ercc1*$^{F/-}$ animals exhibit metabolic abnormalities that are associated with type 2 diabetes mellitus.

Scanning electron microscopy of epididymal WAT and BAT derived from 15-day-old *Ercc1*$^{-/-}$ and WT animals revealed no apparent differences (Figures 2E and S2I). Both *Ercc1*$^{-/-}$ and WT adipose depots show areas of dense cilia formation, characteristic of adipogenic differentiation during development (Satir et al., 2010) (Figure 2E, embedded magnification). Likewise, the 1.5-month-old aP2-*Ercc1*$^{F/-}$ and aP2-*Ercc1*$^{F/+}$ white adipocytes appeared healthy, with spherical and unilocular lipid depots (Figure 2F, as shown). In contrast, the WAT of 4-month-old aP2-*Ercc1*$^{F/-}$ animals showed focal areas of ruptured basal membrane (Figure 2Fi) and frequent loss of adipocytes (Figure 2Fii); red blood cells were sporadically found to occupy empty adipocyte cavities, likely marking the former presence of adipocyte-associated capillaries (Figure 2Fii, embedded magnification). Staining with platelet endothelial cell adhesion molecule 1 (PECAM-1) revealed a dense and well-structured vasculature in aP2-*Ercc1*$^{F/-}$ WAT samples compared to controls (Figure S2L). We also found areas of cilia recurrence in the WAT of 4-month-old aP2-*Ercc1*$^{F/-}$ animals (Figure 2Fiii, embedded magnification). None of these pathological features were seen in the 4-month-old aP2-*Ercc1*$^{F/+}$ WAT depots (Figure S2J). Unlike the aP2-*Ercc1*$^{F/+}$ controls (Figures S2I and S2J), we noticed the presence of excessive interstitial fibrosis at sites of tissue damage in 4-month-old aP2-*Ercc1*$^{F/-}$ animals (Figures 2Fiv and 2G). Together, these findings resemble the pathological abnormalities seen in progressive lipodystrophies ultimately leading to severe metabolic and physiologic abnormalities (Hegele et al., 2007).

Transcriptome Analysis of Epididymal WAT Depots in *Ercc1*$^{-/-}$ Animals

To further elucidate the role of ERCC1 in WAT, we scanned the transcriptome of 15-day-old WT and *Ercc1*$^{-/-}$ epididymal WAT (n = 4). Two-way ANOVA of Affymetrix mouse genome arrays revealed 2,254 genes with significantly changed expression patterns between the *Ercc1*$^{-/-}$ and WT fat depots ($p \leq 0.05$, fold change $\geq \pm 1.2$; Table S1). Using the set of 2,254 genes, we identified the gene ontology (GO)-classified biological processes with a significantly disproportionate number of responsive genes relative to those printed on microarrays (false detection rate ≤ 0.10). This approach revealed five biological processes involved in the response to DNA ICLs and double-strand breaks (DSBs), proinflammatory signaling, nuclear receptor and growth factor signaling, as well as a response to oxidative stress (Figure 3A). These transcriptional changes represent genuine changes in gene regulation as well as reflect a decrease in the fraction of adipocytes relative to stromal cells in *Ercc1*$^{-/-}$ WAT depots. *Ppar*$\gamma^{ldi/+}$ animals carry a targeted allele that confers conditional dominant lipodystrophy in mice (Kim et al., 2007). We therefore compared the gene expression profiles of 10-week-old *Ppar*$\gamma^{ldi/+}$ and P15 *Ercc1*$^{-/-}$ gonadal fat pads. Despite the big difference in age between the two different animal models, we found 768 genes that changed significantly in WAT of both *Ppar*$\gamma^{ldi/+}$ and *Ercc1*$^{-/-}$ mice relative to their WT counterparts. This reflects 34% of the genes significantly altered in *Ercc1*$^{-/-}$ WAT compared to WT mice. Of these, 456 genes (20%) in *Ppar*$\gamma^{ldi/+}$ gonadal fat depots also shared the same direction in expression (Figure 3B; Table S2). Interestingly, we find that PPARγ2, but not PPARγ1, protein and mRNA levels are reduced in the 4-month-old aP2-*Ercc1*$^{F/-}$ animals (Figures 3C–3E and S3A). With the exception of the response to DNA ICLs and DSBs, which was seen exclusively in *Ercc1*$^{-/-}$ mice, the set of 456 genes also found in *Ppar*$\gamma^{ldi/+}$ fat depots was associated with the same overrepresented biological themes identified in *Ercc1*$^{-/-}$ fat pads (Figure 3F). Quantitative PCR (qPCR) and protein immunofluorescence analysis confirmed the validity of these results (Figures 4A and 4B). Taken together, these findings reveal that a gene expression signature of lipodystrophic fat is established early in *Ercc1*$^{-/-}$ progeroid mice.

A Defect in *Ercc1*$^{-/-}$ WAT Depots Triggers Accumulation of γ-H2A.X, RAD51, and FANCI Foci in aP2-*Ercc1*$^{F/-}$ Gonadal Fat Pads

During NER, XPF-ERCC1 makes a single-strand nick near the lesion, which is critical for excision of the damage and thought

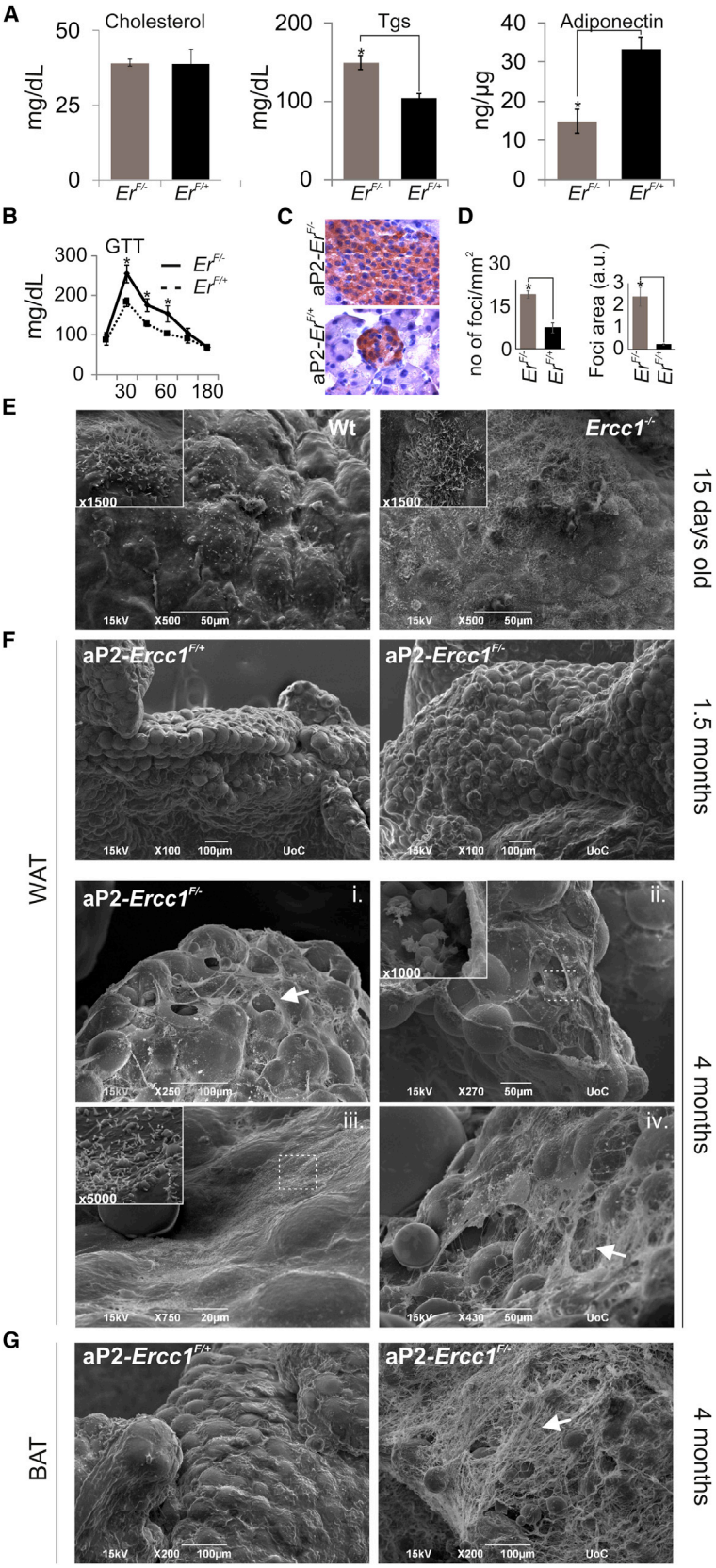

Figure 2. Progressive Lipodystrophy in aP2-*Ercc1*$^{F/-}$ Mice

(A) Serum cholesterol, triglycerides (TGs), and white adipose tissue adiponectin levels of 4-month-old aP2-*Ercc1*$^{F/-}$ (*Er1*$^{F/-}$) and aP2-*Ercc1*$^{F/+}$ (*Er1*$^{F/+}$) animals (n = 4, as indicated).

(B) Glucose tolerance test (GTT) in 4-month-old aP2-*Ercc1*$^{F/-}$ (*Er1*$^{F/-}$) and aP2-*Ercc1*$^{F/+}$ (*Er1*$^{F/+}$) animals (n = 4).

(C) Immunohistochemical analysis of 4-month-old aP2-*Ercc1*$^{F/-}$ (*Er1*$^{F/-}$) and aP2-*Ercc1*$^{F/+}$ (*Er1*$^{F/+}$) pancreata showing staining of β cells, using insulin antibody.

(D) Estimates of number and area of pancreatic islets stained for insulin in the 4-month-old aP2-*Ercc1*$^{F/-}$ (*Er1*$^{F/-}$) and aP2-*Ercc1*$^{F/+}$ (*Er1*$^{F/+}$) animals (n = 4, as indicated).

(E) Representative scanning electron micrographs of 15-day-old WT and *Ercc1*$^{-/-}$ perigonadal white adipose tissue (WAT) depots. Insert: higher magnification indicating cilia in both tissues.

(F) Representative scanning electron micrographs of 1.5-month-old aP2-*Ercc1*$^{F/+}$ and aP2-*Ercc1*$^{F/-}$ WAT depots (upper panel) and 4-month-old aP2-*Ercc1*$^{F/-}$ WAT depots (lower panels). Note the (i) basement membrane rupture, (ii) adipocyte depletion (index: presence of red blood cells indicating capillary destruction), (iii) reappearance of ciliae, and (iv) extensive fibrosis.

(G) Representative scanning electron micrographs of 4-month-old aP2-*Ercc1*$^{F/+}$ and aP2-*Ercc1*$^{F/-}$ brown adipose tissue (BAT) depots. Note the extensive fibrosis in aP2-*Ercc1*$^{F/-}$ BAT depots. *$p \leq 0.05$; a.u., arbitrary units; error bars indicate SEM ($n \geq 3$). See also Figure S2.

A

Overrepresented Pathways	p	R
Response to DNA DSBs		
ATM Signaling	3.75	0.30
Response to DSBs by HR	3.65	0.28
G2/M DNA Damage Checkpoint	2.33	0.25
Proinflammatory signaling		
TNF receptor Signaling	2.89	0.24
Interleukin Signaling	2.44	0.20
NF-kappa B Signaling	2.14	0.18
nNOS Signaling	1.53	0.16
Nuclear Receptor signaling		
PPAR Signaling	2.00	0.19
RAR Activation	1.68	0.16
Transcr/nal Repression Signaling	1.53	0.26
Growth factor signaling		
mTOR Signaling	4.72	0.21
EGF Signaling	2.53	0.25
PI3K/AKT Signaling	2.20	0.17
Insulin Receptor Signaling	2.12	0.18
Response to Stress		
HMGB1 Signaling	3.53	0.24
NRF2 Oxidative Stress Response	2.93	0.19

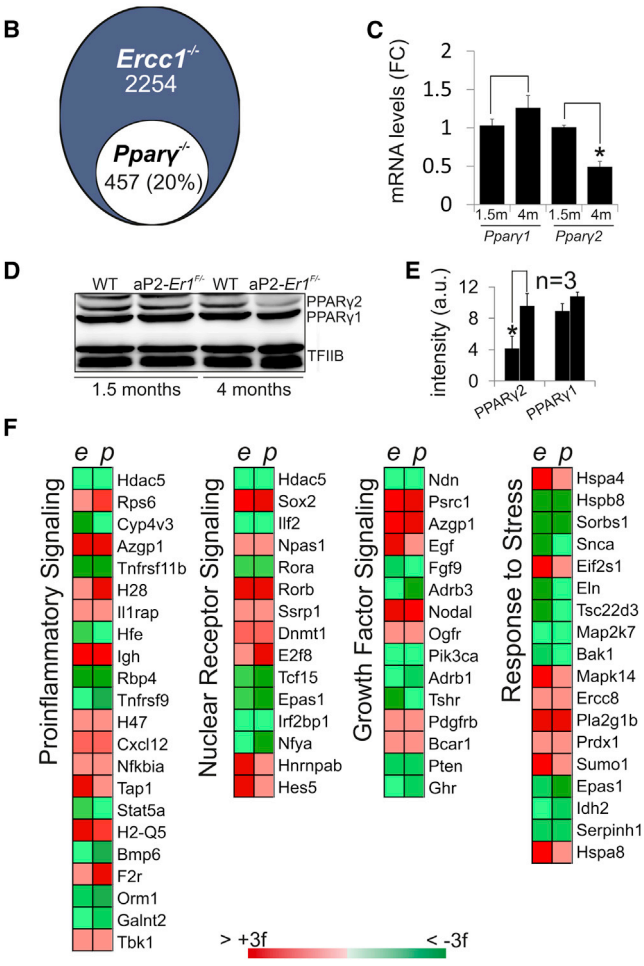

Figure 3. Transcriptome Analysis of Perigonadal WAT Depots in *Ercc1*$^{-/-}$ Mice

(A) Overrepresented biological processes in *Ercc1*$^{-/-}$ perigonadal white adipose tissue (WAT) depots compared to age-matched WT mice. p: −log of p value, which is calculated by Fisher's exact test (right-tailed); R: ratio of number of genes in the indicated pathway divided by the total number of genes that make up that pathway.

(B) Venn diagram representing genes with shared expression changes between *Ercc1*$^{-/-}$ and *Pparγ*$^{ldi/-}$ WAT depots.

(C) mRNA levels of *Pparγ1* and *Pparγ2* in 1.5- and 4-month-old aP2-*Ercc1*$^{F/-}$ WAT depots, compared to age-matched aP2-*Ercc1*$^{F/+}$controls, which were set to 1. The graphs represent the average from 4 mice ± SEM. *p ≤ 0.05 using a two-tailed Student's t test.

(D and E) Western blot (D) and quantification (E) of protein levels of PPARγ1 and PPARγ2 in 1.5- and 4-month-old aP2-*Ercc1*$^{F/+}$ and aP2-*Ercc1*$^{F/-}$ WAT depots.

(F) Heatmap representation of significant gene expression changes between *Ercc1*$^{-/-}$(*e*) and *Pparγ*$^{ldi/-}$(*p*) WAT depots. Data represent the average of 3 mice ± SEM. *p ≤ 0.05 using a two tailed Student's t test. See also Figure S3, Table S1, and Table S2.

to play an analogous role in DNA ICL repair (Niedernhofer et al., 2004). In line with the upregulation of genes associated with the repair of DNA ICLs and DSBs in *Ercc1*$^{-/-}$ WAT depots, several genes associated with the repair of DNA ICLs and DSBs showed increased mRNA levels in 4-month-old, but not 1.5-month-old aP2-*Ercc1*$^{F/-}$ WAT depots (Figure 4A). Phosphorylated histone H2A.X (γ-H2A.X)-containing foci accumulate at sites of DNA breaks (Fernandez-Capetillo et al., 2004). γ-H2A.X staining of aP2-*Ercc1*$^{F/-}$ adipocytes revealed a punctuate pattern of foci; γ-H2A.X gradually accumulated from 1–2 foci/nucleus in the 1.5-month-old animals (~20% positive cells; data not shown) to approximately 3 or more foci/nucleus in the 4-month-old gonadal fat depots (~56% positive cells; Figures 4B and S3C). Similarly, RAD51, a protein involved in the repair of DSBs by homologous recombination (HR) (Elliott and Jasin, 2002), and FANCI, involved in the repair of DNA ICLs (Sato et al., 2012), also formed foci that gradually increased from 1–2 foci/nucleus in the 1.5-month-old mice to >10 foci/nucleus in 4-month-old aP2-*Ercc1*$^{F/-}$ animals (Figures 4B and S3C). Similar to others (Yang et al., 2011; Yang and Kastan, 2000), we found phosphorylated ATM to be predominantly cytoplasmic in adipocytes of 4-month-old aP2-*Ercc1*$^{F/-}$ mice (Figures 4B and S3C). Staining with caspase-3 revealed few, if any, apoptotic cells in 1.5- and 4-month-old aP2-*Ercc1*$^{F/-}$ gonadal fat pads (data not shown). Instead, staining with TO-PRO-3, a carbocyanine monomer nucleic acid stain, revealed a significant increase in necrotic cells (15.4%) in 4-month-old aP2-*Ercc1*$^{F/-}$ WAT depots compared to age-matched controls or to 1.5-month-old aP2-*Ercc1*$^{F/-}$ animals (Figures 4C and S3C). Damage-associated molecular pattern (DAMP) molecules are released by stressed cells undergoing necrosis that act as endogenous danger signals to promote and exacerbate defense responses, including inflammation (Miyake and Yamasaki, 2012). In 4-month-old aP2-*Ercc1*$^{F/-}$ WAT, we detected the release of high-mobility group protein B1 (HMGB1), a central mediator of senescent phenotypes (Davalos et al., 2013) that is associated with DAMPs and is known to initiate and perpetuate immune responses in the noninfectious inflammatory response at sites of injury (Figure 4D) (Miyake and Yamasaki, 2012). HMGB1 protein levels were elevated in 4-month-old aP2-*Ercc1*$^{F/-}$ WAT depots compared to those from age-matched WT mice or 1.5-month-old mice (Figure 4E). Thus, tissue-specific ablation of the *Ercc1* gene triggers the gradual accumulation of persistent cytotoxic DNA damage, which in turn causes

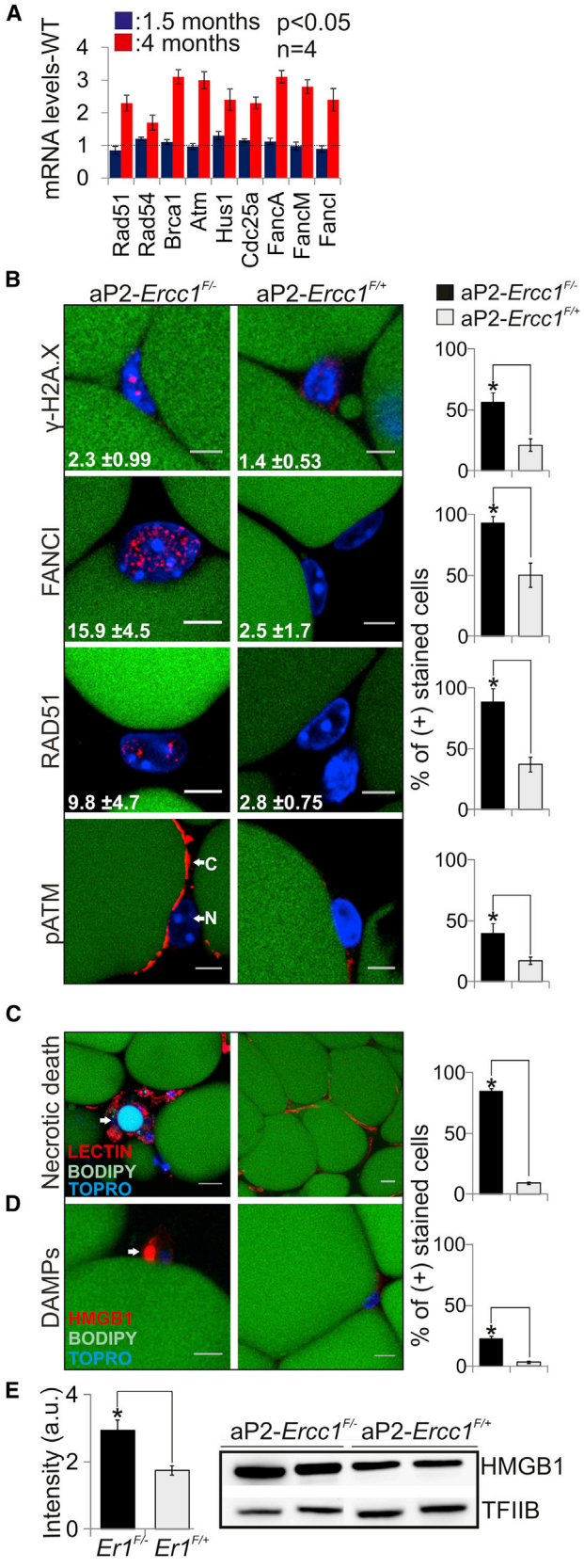

Figure 4. The *Ercc1* Defect Triggers a Response to DNA ICLs and DSBs in aP2-*Ercc1*$^{F/-}$ Fat Depots

(A) qPCR mRNA levels of genes associated with a response to DNA ICLs and DSBs in 1.5- and 4-month-old aP2-*Ercc1*$^{F/-}$ perigonadal white adipose tissue (WAT) depots. Black dotted line: WT mRNA levels.

(B) Immunofluorescence detection of γ-H2A.X, FANCI, RAD51, and pATM foci in aP2-*Ercc1*$^{F/-}$ and aP2-*Ercc1*$^{F/+}$ WAT depots. Note the cytoplasmic localization of pATM foci. Graphs show the percent of positively stained cells ± SD (n = 3). Lower number depicts the average number of foci per cell ± SD.

(C) Immunofluorescence detection of TO-PRO 3 in nonpermeabilized cells, indicating necrotic cell death.

(D) HMGB1 release from chromatin in 4-month-old aP2-*Ercc1*$^{F/-}$ and aP2-*Ercc1*$^{F/+}$ WAT depots. Graphs show the percent of positively stained cells ± SD.

(E) Western blot levels of HMGB1 in 4-month-old aP2-*Ercc1*$^{F/-}$ and aP2-*Ercc1*$^{F/+}$ WAT depots. N, nucleus; C, cytoplasm. Error bars indicate SEM among replicates of three or more animals. Scale bars: b = 5 μm, c = 50 μm, d = 20 μm. *p ≤ 0.05; a.u., arbitrary units. See also Figure S3.

necrotic cell death and the release of DAMPs on the surface of damaged adipocytes in vivo.

Persistent DNA Damage Triggers Chronic Inflammation in Adipose Tissue

The adipose tissue may host macrophages, which accumulate in so-called crown-like structures (CLS) surrounding necrotic adipocytes (Murano et al., 2008). Unlike the 4-month-old WT or the younger 1.5-month-aP2-*Ercc1*$^{F/-}$ animals, confocal imaging of whole-mount 4-month-old aP2-*Ercc1*$^{F/-}$ WAT revealed the presence of bromodeoxyuridine (BrdU$^+$) cells in CLS (Figures 5B and S4A) and infiltrating cells expressing macrophage antigens 1 (MAC1$^+$) and 3 (MAC3$^+$) that formed syncytia around dying adipocytes (Figures 5B and S4B). Both proteins are essential for leukocyte activation, and MAC3 is a marker of differentiated macrophages (Khazen et al., 2005). Total white blood cell (WBC) counts and fluorescence-activated cell sorting (FACS) analysis in 4-month-old aP2-*Ercc1*$^{F/-}$ animals also revealed a significant increase in the number of WBCs and an increase of CD11b$^+$- and CD11c$^+$-stained cells in the stromal vascular fraction, marking the presence of macrophages in these animals (Figures 5C, S4C, and S4D). MAC1$^+$ cells in 4-month-old aP2-*Ercc1*$^{F/-}$ fat depots expressed inducible nitric oxide synthase (iNOS), a potent inducer of chronic inflammation and a marker of activated macrophages (M1 type); CD45, a marker of leukocytes; and two endothelial adhesion molecules, ICAM-1 and VCAM, which are known to facilitate the accumulation of monocytes at sites of tissue injury (Figure 5D). ELISA assay on fat tissue revealed interleukin-6 (IL-6), tumor necrosis factor alpha (TNF-α), and KC (murine homolog to IL-8) protein levels to be elevated in the 4-month-old aP2-*Ercc1*$^{F/-}$ WAT depots compared to controls (Figure 5E). Similar data were found for TNF-α and KC protein levels in the 4-month-old aP2-*Ercc1*$^{F/-}$ sera; IL-6 was undetectable (Figure S4F). Similarly, *Il6*, *Tnfα*, and *Kc* mRNA levels were increased in the adipose tissue of 4-month-old aP2-*Ercc1*$^{F/-}$ animals compared to younger mice of the same genotype (Figure 5E, as indicated). As infiltrating macrophages could also express proinflammatory cytokines, we also analyzed the expression of *Il6*, *Tnfα*, and *Kc* mRNA levels in the stromal vascular and the adipocyte-rich fractions of 4-month-old aP2-*Ercc1*$^{F/-}$ and aP2-*Ercc1*$^{F/+}$ WAT depots. Although increased expression of proinflammatory cytokines

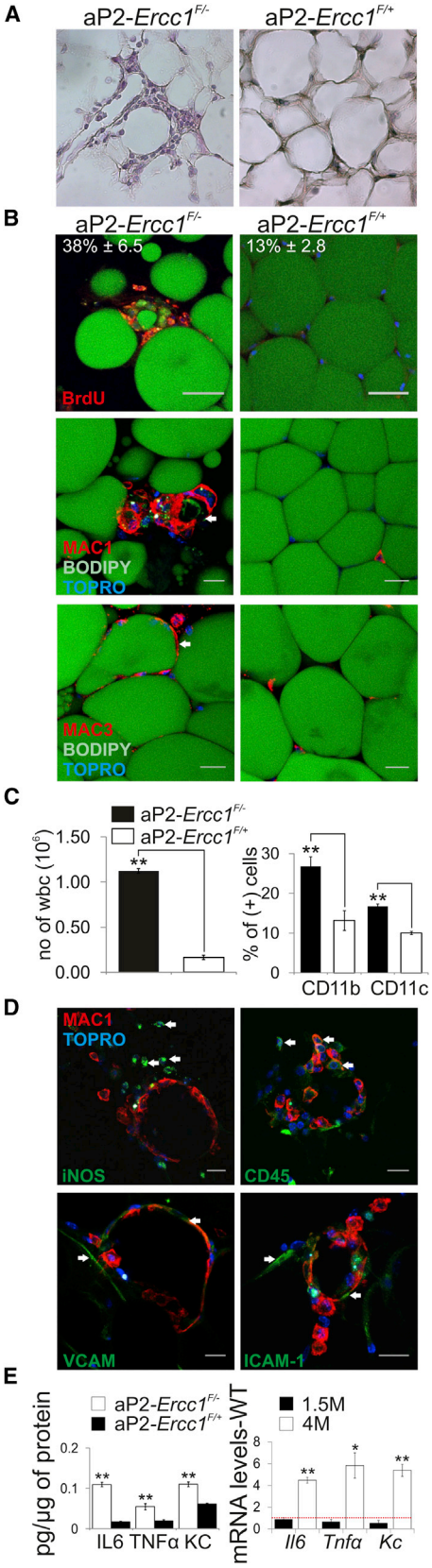

Figure 5. Tissue-Specific Ablation of ERCC1 Triggers an Inflammatory Response in aP2-*Ercc1*$^{F/-}$ Adipose Tissue Depots

(A) Hematoxylin and eosin (H&E) staining of 4-month-old aP2-*Ercc1*$^{F/-}$ perigonadal white adipose tissue (WAT) depots indicating the formation of crown-like structures (CLS) compared to aP2-*Ercc1*$^{F/+}$ controls.

(B) Confocal imaging of whole-mount aP2-*Ercc1*$^{F/-}$ WAT, indicating the presence of BrdU^{+} cells in CLS and infiltrating MAC1^{+} and MAC3^{+} macrophages forming syncytia around dying adipocytes as compared to aP2-*Ercc1*$^{F/+}$ controls.

(C) Number of white blood cells (wbc) per gram of tissue and percent of CD11b (+) and CD11c (+) stained cells in the stromal vascular fraction of 4-month-old aP2-*Ercc1*$^{F/-}$ and aP2-*Ercc1*$^{F/+}$ animals (as indicated).

(D) Confocal imaging of whole-mount aP2-*Ercc1*$^{F/-}$ WAT, indicating the presence of MAC1(+) cells expressing proinflammatory molecules iNOS, CD45, and monocyte-attracting cell adhesion ICAM-1 and VCAM molecules in the CLS (as indicated).

(E) Protein (left) and mRNA (right) levels of IL-6, TNFα, and KC measured by whole-tissue ELISA and qPCR, respectively, in the WAT of 4-month-old aP2-*Ercc1*$^{F/-}$ mice and aP2-*Ercc1*$^{F/+}$ controls. Scale bars: 20 μm; error bars indicate SEM among replicates ($n \geq 3$); *$p \leq 0.05$, **$p \leq 0.01$. See also Figure S4.

was documented in both aP2-*Ercc1*$^{F/-}$ fractions compared to aP2-*Ercc1*$^{F/+}$ controls, the *Il6*, *Tnf*α, and *Kc* mRNA levels were substantially higher in the adipocyte-rich fraction compared to the stromal vascular fraction (Figure S4E). Similar data were found in *Ercc1*$^{\Delta/-}$ animals carrying a seven amino acid carboxy-terminal deletion in the *Ercc1* gene (Weeda et al., 1997). Nine-week-old *Ercc1*$^{\Delta/-}$ animals showed a substantial loss of WAT depots (n = 9); we also found increased IL-6, TNF-α, and KC protein levels in the 9- and 20-week-old *Ercc1*$^{\Delta/-}$ WAT depots as well as in the 20-week-old *Ercc1*$^{\Delta/-}$ WAT depots at the mRNA level relative to control animals (n = 4; Figures S4G–S4J). Together, our findings show that the formation of DNA damage foci correlates with the onset of proinflammatory signals in aP2-*Ercc1*$^{F/-}$ fat depots; the proinflammatory response is initiated by adipocytes rather than by infiltrating macrophages to necrotic adipocytes.

ICLs Induce a Proinflammatory Response in Adipocytes

Next, we used an ex vivo adipogenic assay to test whether DNA damage directly contributes to proinflammatory cytokine production in adipocytes. Naive primary WT and *Ercc1*$^{-/-}$ mouse embryonic fibroblasts (MEFs) were exposed to an adipogenic stimulus for 13 days. This led to the de novo lipid accumulation marking the generation of differentiated, functional adipocytes expressing adipocyte-specific markers, including *Cebp4*, *Fabp4*, *Adiponectin*, and *Adipsin* genes (Figure S5A). Unlike the WT adipocytes or undifferentiated *Ercc1*$^{-/-}$ MEFs, *Ercc1*$^{-/-}$ adipocytes showed a dramatic accumulation of spontaneous γ-H2A.X, pATM, and FANCI, but not RAD51, foci (Figures 6A and S5B). In addition, *Ercc1*$^{-/-}$ adipocytes showed increased *Tnf*α, *Il6*, and *Kc* mRNA levels compared to WT adipocytes when each was compared to undifferentiated controls (Figure 6B, as indicated). Thus, irreparable DNA lesions in otherwise unchallenged *Ercc1*$^{-/-}$ adipocytes trigger the production of proinflammatory factors. To further test this, we treated WT adipocytes with mitomycin C (MMC), a potent inducer of DNA crosslinks, for 2 hr. This led to an increase in *Tnf*α, *Il6*, and *Kc* mRNA levels (Figure 6B, as indicated); similar to our previous findings (Figure 6B), the increase in proinflammatory cytokine mRNA levels was substantially higher in MMC-treated

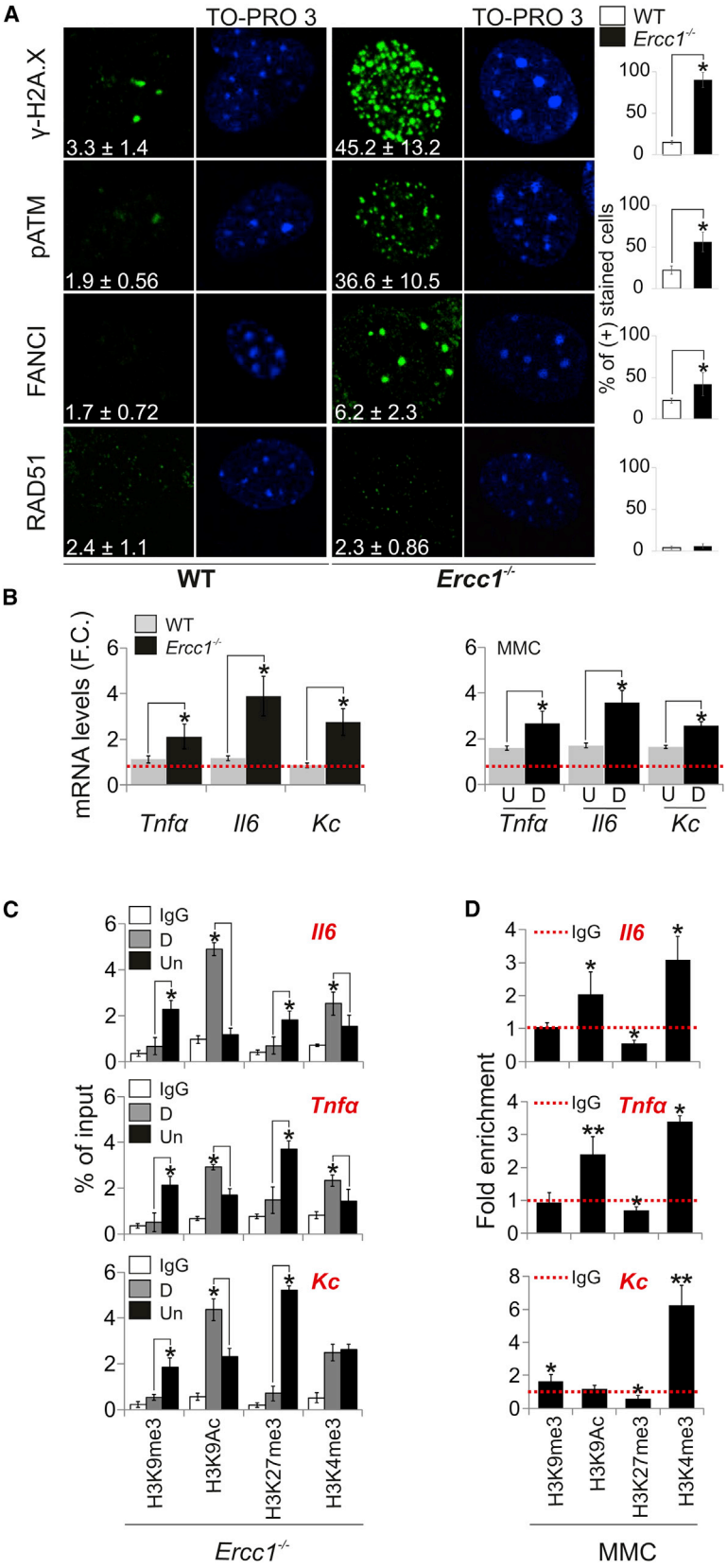

Figure 6. Accumulation of Persistent DNA ICLs Leads to Histone PTMs Associated with Active Transcription of Proinflammatory Cytokines

(A) Immunofluorescence detection of γ-H2A.X, pATM, FANCI, and RAD51 proteins in WT and *Ercc1*$^{-/-}$ mouse embryonic fibroblasts (MEFs) exposed to the adipogenic stimulus (D, differentiated). Note the accumulation of γ-H2A.X, pATM, and FANCI, but not of RAD51, nuclear foci in *Ercc1*$^{-/-}$ adipocytes. The number at the bottom depicts the average number of foci per cell ± SD from 20 fields analyzed from 3 or more cell cultures.

(B) qPCR mRNA levels of *Tnfα*, *Il6*, and *Kc* proinflammatory cytokines in *Ercc1*$^{-/-}$ or WT adipocytes as compared to MEFs (left) and in mitomycin C (MMC)-treated WT adipocytes (D) or MEFs (U) as compared to non-MMC-treated WT adipocytes or MEFs, respectively (right).

(C) ChIP signals (shown as percent of input) of repressive H3K9me3, H3K27me3, activating H3K9Ac, H3K4me3 histone marks, and immunoglobulin G (IgG) control at the *Il6*, *Tnfα*, and *Kc* proximal promoter regions in adipocytes or MEFs carrying the Ercc1 defect (*Ercc1*$^{-/-}$). Error bars indicate SEM among replicates ($n \geq 3$).*$p \leq 0.05$.

(D) ChIP signals (shown as fold enrichment) of repressive H3K9me3, H3K27me3, activating H3K9Ac, and H3K4me3 histone marks at the *Il6*, *Tnfα*, and *Kc* proximal promoter regions in WT adipocytes exposed to MMC as compared to untreated controls. ChIP signals were normalized to input and expressed as fold enrichment over those obtained with control antibody (IgG), which were set as 1 (red dotted line). D, differentiated; U, undifferentiated. Error bars indicate SEM among replicates ($n \geq 3$). *$p \leq 0.05$. See also Figure S5.

adipocytes than in MEFs relative to corresponding untreated controls. As the aP2 promoter selected in our work has been reported to be expressed also in macrophages (Mao et al., 2009), we tested whether *Ercc1* expression is compromised in macrophages at the origin of the phenotype observed in aP2-*Ercc1*$^{F/-}$ WAT depots. We find *Ercc1* levels in macrophages to be comparable at both the mRNA and the protein levels in the 2.5-month-old aP2-*Ercc1*$^{F/-}$ compared to aP2-*Ercc1*$^{F/+}$ animals (Figures S1K–S1M). Taken together, our findings suggest that the transcription activation of proinflammatory cytokines is cell autonomous; it requires the presence of persistent DNA damage foci and is exacerbated in adipocytes compared to undifferentiated MEFs.

DNA Damage Signaling Triggers Histone Changes Associated with Active Transcription on Promoters

To gain further mechanistic insight into how the accumulation of persistent DNA damage foci leads to the transcriptional activation of *Tnfα*, *Il6*, and *Kc* in *Ercc1*$^{-/-}$ adipocytes, we carried out a series of chromatin immunoprecipitation (ChIP) assays to examine the status of *Il6*, *Tnfα*, and *Kc* promoters. Our analysis revealed loss of repressive histone H3K9 and H3K27 trimethylation marks and an increase of activating acetylated histone H3K9 and H3K4 trimethylation marks in *Ercc1*$^{-/-}$ adipocytes compared to *Ercc1*$^{-/-}$ MEFs. Similar data were seen in MMC-treated WT adipocytes compared to untreated controls (Figures 6C and 6D). WT adipocytes also displayed an increase in activating histone marks compared to undifferentiated MEFs; however, unlike the *Ercc1*$^{-/-}$ adipocytes, repressive histone H3K9 and H3K27 trimethylation marks were maintained or increased in these cells (data not shown). Thus, a defect in DNA repair of spontaneous DNA damage or exposure of adipocytes to the genotoxin MMC triggers posttranslational modifications of histones associated with active transcription in *Il6*, *Tnfα*, and *Kc* gene promoters.

Persistent DNA Damage Signaling Triggers the Transcriptional Derepression of *Il6*, *Tnfα*, and *Kc*

There is mounting evidence that at least some proinflammatory cytokines are in a poised, yet repressed, transcriptional state. Repression of active transcription is mediated by the recruitment of a corepressor complex containing the nuclear receptor corepressor (NCoR1) or the related silencing mediator of retinoic acid and thyroid hormone receptors (SMRT) on promoters (Perissi et al., 2010). PPARγ, whose protein and mRNA levels were substantially decreased in aP2-*Ercc1*$^{F/-}$ WAT depots, recruits SMRT and NCoR1 in the absence of ligands, and these corepressors are capable of downregulating PPARγ-mediated transcriptional activity. In addition, NCoR1 and SMRT mediate active repression of their respective target genes through the recruitment of additional corepressor molecules, including the histone deacetylase HDAC3 (Perissi et al., 2010). Importantly, exposure of WT adipocytes to MMC led to the suppression of *Pparγ2*, but not *Pparγ1*, mRNA levels (Figure S3B). This and the upregulation of *Il6*, *Tnfα*, and *Kc* proinflammatory cytokine mRNA levels in *Ercc1*$^{-/-}$ fat depots prompted us to examine whether the corepressor complex NCoR1-SMRT-HDAC3 is released from promoters in *Ercc1*$^{-/-}$ adipocytes or upon exposure of WT adipocytes to MMC. With the exception of NCoR1 for *Tnfα* promoter in *Ercc1*$^{-/-}$ adipocytes, we found substantially lower ChIP signals for NCoR1, SMRT, and HDAC3 on *Il6*, *Tnfα*, and *Kc* promoters of *Ercc1*$^{-/-}$ adipocytes or MMC-treated WT adipocytes relative to corresponding controls (Figure 7A); intriguingly, we also found *Pparγ2*, but not *Pparγ1*, mRNA levels to be substantially reduced in WT adipocytes exposed to MMC, suggesting a functional link between DNA damage and the transcriptional downregulation of nuclear receptors in adipocytes (Figure S3B). Thus, defective DNA repair or exposure of WT adipocytes to a crosslinking agent triggers the transcriptional derepression of proinflammatory cytokines.

The accumulation of ATM foci in the cytoplasm of 4-month-old aP2-*Ercc1*$^{F/-}$ adipocytes prompted us to test whether ATM is required for the DNA damage-driven transcriptional derepression of *Il6*, *Tnfα*, and *Kc* in adipocytes. Inactivation of ATM by exposing MMC-treated adipocytes to KU-55933 inhibitor (known to ablate DNA damage-induced phosphorylation of ATM substrates) (Ding et al., 2006) significantly abrogated the release of repressor complexes from promoters and abolished the transcriptional induction of *Il6*, *Tnfα*, and *Kc* mRNA levels in these cells (Figure 7B). We also exposed MMC-treated adipocytes to ATR/CDK inhibitor NU6027, known to inhibit ATR kinase without interfering with irradiation-induced autophosphorylation of DNA-dependent protein kinase (DNA-PK) or ATM. Inactivation of ataxia telangiectasia and Rad3-related protein (ATR) led results similar to those seen upon ATM inactivation, albeit to a smaller magnitude (Figure 7B). Thus, while ATR may contribute to the transcriptional derepression of promoters, ATM is essential in linking the nuclear DDR signaling to the transcriptional activation of proinflammatory cytokines in aP2-*Ercc1*$^{F/-}$ WAT depots. Similarly, activation of the antiinflammatory PPARγ by exposing MMC-treated adipocytes to rosiglitazone, a PPARγ agonist, significantly abrogated the transcriptional induction of *Il6*, *Tnfα*, and *Kc* mRNA levels (Figure 7B). To test whether ATM and PPARγ play similar roles in *Ercc1*$^{-/-}$ adipocytes, we inhibited ATM or activated PPARγ in *Ercc1*$^{-/-}$ adipocytes; importantly, treatment of *Ercc1*$^{-/-}$ adipocytes with KU-55933 inhibitor or rosiglitazone significantly abrogated the transcriptional induction of *Il6*, *Tnfα*, and *Kc* mRNA levels compared to untreated controls (Figure 7C), a finding that was also confirmed in ATM inhibitor (ATMi)-treated adipocyte culture media for TNF-α protein levels (Figure S5D). Finally, we found that *Ercc1* mRNA levels are significantly decreased, whereas *Il6*, *Tnfα*, and *Kc* mRNA levels are significantly increased in 110-week-old compared to 6-week-old WT fat depots (Figure S5C). Thus, our findings provide a model in which persistent DNA damage in aP2-*Ercc1*$^{-/-}$ fat depots in vivo and in adipocytes ex vivo triggers the induction of proinflammatory cytokines by promoting transcriptionally active histone marks and the dissociation of nuclear receptor corepressor complexes from promoters (Figure 7C).

DISCUSSION

How DNA damage triggers the onset of tissue-specific pathology in NER patients and accompanying mouse models remains an intriguing question asking for tissue-specific responses against deleterious threats. Besides cachectic dwarfism, *Ercc1*$^{-/-}$ mice show several progeroid features, including the noticeable loss of adipose tissue depots. To distinguish between

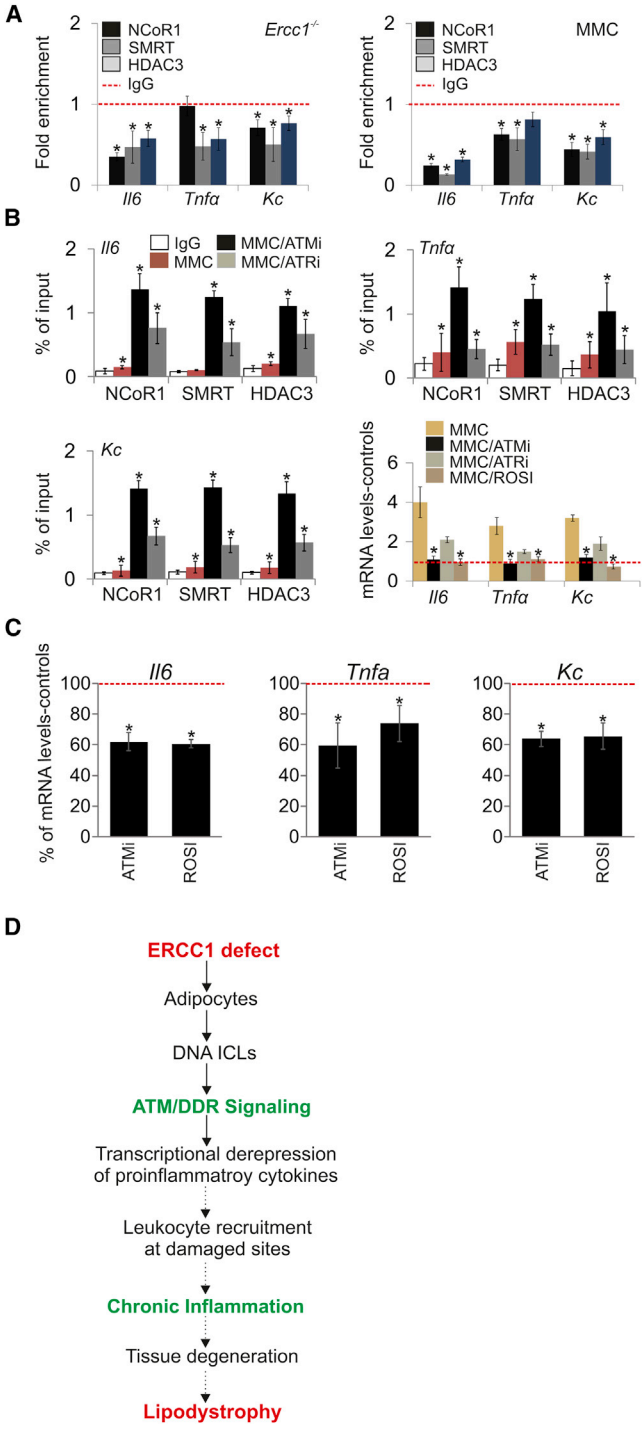

Figure 7. Persistent ICLs Trigger the Transcriptional Derepression of Proinflammatory Cytokines

(A) ChIP signals of the nuclear receptor corepressors NCoR1, SMRT, and HDAC3 on promoters of proinflammatory cytokines in *Ercc1*$^{-/-}$ adipocytes (shown in left) and WT MMC-treated adipocytes (right) as compared to corresponding, undifferentiated controls (n = 3). ChIP signals were normalized to input and expressed as fold enrichment over those obtained with control antibody (IgG), which were set as 1 (red dotted line). *p $\leq$ 0.05.

(B) ChIP signals of the nuclear receptor corepressors NCoR1, SMRT, HDAC3, and IgG control on promoters of proinflammatory cytokines in WT MMC-treated adipocytes in the presence or absence of ATM (ATMi) and ATR (ATRi) kinase inhibitors (as shown). qPCR mRNA levels of *Il6*, *Tnfα*, and *Kc* in MMC-treated adipocytes exposed to the ATM (ATMi) and ATR (ATRi) kinase inhibitors (as shown).

(C) qPCR mRNA levels of *Il6*, *Tnfα*, and *Kc* in *Ercc1*$^{-/-}$ adipocytes exposed to ATM inhibitor (ATMi) and Rosiglidazone as compared to nontreated *Ercc1*$^{-/-}$ adipocytes (as shown).

(D) Schematic representation of the causal relationship between the ERCC1 deficiency, persistent DDR signaling, and adipose tissue degeneration in DNA repair-defective animals. Data are represented as mean ± SEM. See also Figure S5.

causative and indirect mechanisms of fat depletion in the ERCC1-deficient mice, we focused our studies on fat-specific aP2-*Ercc1*$^{F/-}$ animals. Because aP2 gene expression does not peak until the adipocyte is mature (Tang et al., 2008), ERCC1 is deleted at a later stage in the aP2-*Ercc1*$^{F/-}$ animals. This allows us to gain insights into the effect of time-dependent accumulation of DNA damage on adult fat depots. Importantly, aP2-*Ercc1*$^{F/-}$ mice are born with Mendelian frequency, grow normally, are fertile, and show no visible pathological signs until adulthood. Beginning at 2.5 months, however, aP2-*Ercc1*$^{F/-}$ mice exhibit marked signs of lipodystrophy, including a considerable decrease in adipocyte size, tissue necrosis and fibrosis in injured sites, as well as metabolic abnormalities that are associated with insulin resistance and diabetes mellitus type 2. Although fat depletion and obesity are opposites in terms of fat mass, both conditions are accompanied by similar metabolic abnormalities, inflammation, and macrophage infiltration into adipose tissue depots; the latter are, however, different in terms of abundance, activation state, and gene expression (Herrero et al., 2010).

Importantly, aP2-*Ercc1*$^{F/-}$ fat depots showed hallmarks of persistent DDR; ATM foci appeared predominantly in the cytoplasm, supporting recent observations that link cytoplasmic ATM with downstream cytokine signaling (Hinz et al., 2010). Persistent DDR foci in aP2-*Ercc1*$^{F/-}$ fat depots appeared together with the upregulation of proinflammatory factors, the infiltration of activated macrophages in CLS, as well as the release of DAMPs, such as HMGB1, that can trigger cytokine release, further propagating the inflammatory response in damaged fat depots (Sims et al., 2010). Thus, persistent DDR signaling closely correlates with inflammatory cytokine production at damaged aP2-*Ercc1*$^{F/-}$ fat depots.

The presence of FANCI foci without RAD51 foci in *Ercc1*$^{-/-}$ adipocytes argues for the presence of irreparable DNA ICLs in these cells; however, as RAD51 is also needed for ICL repair, our findings suggest that ICL damage signaling is activated, but in the absence of incision by ERCC1-XPF, DNA repair cannot take place, hence the absence of HR foci. The lack of DDR foci formation in unchallenged *Ercc1*$^{-/-}$ MEFs (as compared to *Ercc1*$^{-/-}$ adipocytes) suggests that certain types of cells (i.e., adipocytes) experience high levels of genotoxic stress. Lipid peroxide is an endogenous source of crosslinking agents (Niedernhofer et al., 2003). In WAT, where lipids are most abundant, inflammation and consequential lipid peroxidation could trigger the formation of more DNA ICLs. This and the inherent propensity of adipocytes to secrete proinflammatory signals upon metabolic stress (Tchkonia et al., 2010) could establish self-perpetuating proinflammatory cycles, leading to systemic

metabolic dysfunction. Unlike the *Ercc1*$^{-/-}$ WAT depots, *Ercc1*$^{-/-}$ cells did not show a cytoplasmic localization of ATM, likely reflecting lineage-specific differences between adipocytes and MEFs exposed to adipogenic differentiation media (Li et al., 2009).

In our work, abrogation of ERCC1 in adipocytes or exposure of WT adipocytes to MMC crosslinking agent led to the transcriptional activation of proinflammatory cytokines in vitro. DNA damage was sufficient to trigger the expression of proinflammatory cytokines whether or not cells were competent to proliferate. Previous studies suggest that human cells induced to senesce by genotoxic stress secrete several proinflammatory factors (Coppé et al., 2008). However, cells induced to senesce by p16INK4a expression, but in the absence of DNA damage, did not initiate a cytokine response (Rodier et al., 2009), further supporting our observations that DDR can independently trigger a proinflammatory response in aP2-*Ercc1*$^{F/-}$ fat depots.

Whereas genes that mediate inflammatory responses must be kept tightly repressed under normal conditions, they must also be rapidly induced in the setting of tissue injury. PPARγ is a nuclear hormone receptor that has potent antiinflammatory roles (Straus and Glass, 2007). The P15 *Ercc1*$^{-/-}$ WAT depots showed decreased PPARγ2 mRNA and protein levels and a considerable overlap in gene expression changes with 10-week-old *Pparγ*$^{ldi/+}$ adult animals. As PPARγ modulates responses by forming protein complexes with coactivators or corepressors on promoters (Guan et al., 2005), we asked whether a similar mechanism could initiate the transition of proinflammatory genes from a repressed to an actively transcribed state in adipocytes. Abrogation of ERCC1 in adipocytes or exposure of WT adipocytes to MMC triggers histone posttranslational modifications that associate with active transcription of proinflammatory factors in adipocytes. Subsequent studies in *Ercc1*$^{-/-}$ and MMC-treated WT adipocytes revealed the dissociation of corepressors NCoR1, SMRT, and HDAC3 from promoters, closely matching the increase of *Il6*, *Tnfα*, and *Kc* mRNA levels in these cells. Importantly, ATM, and to a lesser extent ATR, inactivation abolished the DNA damage-driven release of corepressor complexes from promoters and the induction of proinflammatory cytokine expression in adipocytes. Thus, the transcriptional derepression of proinflammatory genes in adipocytes requires DDR signaling, with active ATM playing a prominent role in mediating the proinflammatory response to persistent genotoxic stress in fat depots.

It has been challenging to delineate how different cell populations respond to DNA damage in vivo and the mechanism by which DNA damage drives tissue-specific pathology in NER progeroid syndromes. Here, we provide evidence for a functional link between persistent DNA damage and loss of fat depots, a feature of accelerated and natural aging. Using mice carrying an adipose tissue-specific defect in ERCC1-XPF DNA repair endonuclease, we provide in vivo evidence that the gradual accumulation of irreparable DNA lesions in *Ercc1*$^{-/-}$ adipocytes triggers a chronic autoinflammatory response leading to adipose tissue degeneration. In the short term, this response would allow damaged cells to communicate their compromised state to the microenvironment; in the long term, however, it leads to age-related degeneration and loss of fat depots.

EXPERIMENTAL PROCEDURES

Animal Studies

Ercc1^{F} mice containing a floxed allele of the *Ercc1* gene (Verhagen-Oldenampsen et al., 2012) and Rosa26-YFP$^{st/st}$ mice were crossed with Fabp4 (aP2)-*Cre* transgenic mice to obtain inactivation of the *Ercc1* gene or expression of YFP in adipocytes, respectively. For insulin and glucose tolerance tests, mice were injected intraperitoneally with 0.75 units/kg of body weight insulin (Humulin; Eli Lilly) or with 1 g/kg of body weight 35% dextrose solution, respectively. For BrdU incorporation studies, mice were injected intraperitoneally with 30 mg/kg of body weight BrdU (Sigma) in 1× PBS and sacrificed 48 hr later. An independent Animal Ethical Committee at the IMBB-FORTH approved the animal studies. Detailed information on experimental procedures is described in the Supplemental Experimental Procedures.

Scanning Electron Microscopy

For scanning electron microscopy, fresh adipose tissue was cut into small blocks and fixed, and specimens were coated in gold, mounted on aluminum stubs, and examined with a JEOL JSM-6390LV Scanning Electron Microscope using an accelerating voltage of 15 kV.

Histology

For lipid staining, OCT-embedded tissues were cryosectioned, fixed in 10% formalin, stained with oil red O, and counterstained with Harris's haematoxylin. For insulin staining, paraffin-embedded pancreata were sectioned, deparaffinized, boiled in 10 mM sodium citrate buffer, stained with anti-insulin antibody (Cell Signaling Technology), and visualized with DAB chromogen (Sigma).

Microarrays and qPCR Assays

Microarrays, qPCR, and qPCR data analysis were performed as previously described (Kamileri et al., 2012b). Primer sequences for the genes tested by qPCR are available upon request.

Immunostaining, Western Blots, ChIP Assays, and Antibodies

Immunofluorescence experiments were performed as previously described (Garinis et al., 2005; Nishimura et al., 2008) and visualized with a Leica TCS SP2 SE Confocal Microscope. For ChIP assays, cells were crosslinked with 1% formaldehyde, chromatin was sonicated using an Ultrasonic Homogenizer, and samples were immunoprecipitated with antibodies and protein G Sepharose beads (Millipore). Purified DNA fragments were analyzed by qPCR using primers targeting different regions of *IL6*, *TNF*, *and KC* genes. Detailed information is provided in the Supplemental Experimental Procedures.

Inflammatory Cell Counts and FACS Analysis

Epididymal adipose tissue fragments were incubated in 1× HEPES-buffered saline (HBS) supplemented with 2 mg/ml Collagenase (Sigma) for 1 hr at 37°C. The stromal vascular fraction was collected by centrifugation, and cells were filtered to obtain single cell suspensions. White blood cell counts per mouse were estimated using Kimura stain (Kimura et al., 1973). To estimate adipose tissue inflammatory cells by FACS analysis, cells were stained with fluorescein isothiocyanate (FITC)-CD11b (BD Biosciences) or FITC-CD11c antibodies (BioLegend). Flow cytometry events were acquired with a MoFlo Legacy Cell Sorter (Beckman Coulter) and analyzed using the Summit Software.

Cell Culture and Ex Vivo Adipogenesis Assays

Primary MEFs 2 days after confluency were induced for adipocyte differentiation with standard medium supplemented with an adipogenic cocktail. Adipocytes and undifferentiated MEFs were treated with 10 μg/μl mitomycin C (AppliChem) for 2 hr in serum-free Dulbecco's modified Eagle's medium (DMEM) and recovered after 6 hr in standard medium. For ATM or ATR kinase inhibitor assays, cells were treated for 1 hr with 10 μM inhibitor (Millipore) followed by the addition of MMC. *Ercc1*$^{-/-}$ MEFs were treated with ATMi for 48 hr or with 0.5 μM rosiglitazone (Santa Cruz) throughout differentiation.

Data Analysis

For microarrays, two-tail, pair-wise analysis or a two-way ANOVA was used to extract the statistically significant gene expression data by means of the IBM

SPSS Statistics 19, Spotfire (TIBCO), Partek (Partek Incorporated), and R-statistical package (www.r-project.org/). Significant overrepresentation of pathways and gene networks was determined by DAVID (http://david.abcc.ncifcrf.gov/summary.jsp; through BBID, BIOCARTA, and KEGG annotations) as well as by means of the ingenuity pathway analysis software (www.ingenuity.com). Detailed information is provided in the Supplemental Experimental Procedures.

ACCESSION NUMBERS

The ArrayExpress accession number for the microarray data reported in this paper is E-MEXP-3930.

SUPPLEMENTAL INFORMATION

Supplemental Information includes Supplemental Experimental Procedures, five figures, and two tables and can be found with this article online at http://dx.doi.org/10.1016/j.cmet.2013.08.011.

ACKNOWLEDGMENTS

This work was supported by Heracleitus II, NSRF-ESPA 2007-2013 (KA3396); Cooperation I, NSRF-ESPA 2007-2013 (901-13/11/2009); GenAge, NSRF-ESPA 2007-2013 (380228); miREG, NSRF-ESPA 2007-2013 (380247); TagNER, NSRF-ESPA 2007-2013 (45); ELKE, University of Crete (901-13/11/2009); the aDDRess, FP7 Marie Curie ITN (316390); CodeAge, FP7 Marie Curie ITN (316354); and Marriage, FP7 Marie Curie ITN (316964). I.K. is supported by the Maria-Michail Manassakis fellowship. A.R.R. and L.J.N. were supported by NIH (ES016114). G.A.G. is supported by the EMBO Young Investigator program. None of the authors of this work have a financial interest related to this work.

Received: January 14, 2013
Revised: May 18, 2013
Accepted: August 9, 2013
Published: September 3, 2013

REFERENCES

Coppé, J.P., Patil, C.K., Rodier, F., Sun, Y., Muñoz, D.P., Goldstein, J., Nelson, P.S., Desprez, P.Y., and Campisi, J. (2008). Senescence-associated secretory phenotypes reveal cell-nonautonomous functions of oncogenic RAS and the p53 tumor suppressor. PLoS Biol. *6*, 2853–2868.

Davalos, A.R., Kawahara, M., Malhotra, G.K., Schaum, N., Huang, J., Ved, U., Beausejour, C.M., Coppe, J.P., Rodier, F., and Campisi, J. (2013). p53-dependent release of Alarmin HMGB1 is a central mediator of senescent phenotypes. J. Cell Biol. *201*, 613–629.

DiGiovanna, J.J., and Kraemer, K.H. (2012). Shining a light on xeroderma pigmentosum. J. Invest. Dermatol. *132*, 785–796.

Ding, J., Miao, Z.H., Meng, L.H., and Geng, M.Y. (2006). Emerging cancer therapeutic opportunities target DNA-repair systems. Trends Pharmacol. Sci. *27*, 338–344.

Elliott, B., and Jasin, M. (2002). Double-strand breaks and translocations in cancer. Cell. Mol. Life Sci. *59*, 373–385.

Fernandez-Capetillo, O., Lee, A., Nussenzweig, M., and Nussenzweig, A. (2004). H2AX: the histone guardian of the genome. DNA Repair (Amst.) *3*, 959–967.

Garinis, G.A., Mitchell, J.R., Moorhouse, M.J., Hanada, K., de Waard, H., Vandeputte, D., Jans, J., Brand, K., Smid, M., van der Spek, P.J., et al. (2005). Transcriptome analysis reveals cyclobutane pyrimidine dimers as a major source of UV-induced DNA breaks. EMBO J. *24*, 3952–3962.

Garinis, G.A., van der Horst, G.T., Vijg, J., and Hoeijmakers, J.H. (2008). DNA damage and ageing: new-age ideas for an age-old problem. Nat. Cell Biol. *10*, 1241–1247.

Guan, H.P., Ishizuka, T., Chui, P.C., Lehrke, M., and Lazar, M.A. (2005). Corepressors selectively control the transcriptional activity of PPARgamma in adipocytes. Genes Dev. *19*, 453–461.

Hanawalt, P.C. (2002). Subpathways of nucleotide excision repair and their regulation. Oncogene *21*, 8949–8956.

Hegele, R.A., Joy, T.R., Al-Attar, S.A., and Rutt, B.K. (2007). Thematic review series: Adipocyte Biology. Lipodystrophies: windows on adipose biology and metabolism. J. Lipid Res. *48*, 1433–1444.

Herrero, L., Shapiro, H., Nayer, A., Lee, J., and Shoelson, S.E. (2010). Inflammation and adipose tissue macrophages in lipodystrophic mice. Proc. Natl. Acad. Sci. USA *107*, 240–245.

Hinz, M., Stilmann, M., Arslan, S.C., Khanna, K.K., Dittmar, G., and Scheidereit, C. (2010). A cytoplasmic ATM-TRAF6-cIAP1 module links nuclear DNA damage signaling to ubiquitin-mediated NF-κB activation. Mol. Cell *40*, 63–74.

Jones, J.R., Barrick, C., Kim, K.A., Lindner, J., Blondeau, B., Fujimoto, Y., Shiota, M., Kesterson, R.A., Kahn, B.B., and Magnuson, M.A. (2005). Deletion of PPARgamma in adipose tissues of mice protects against high fat diet-induced obesity and insulin resistance. Proc. Natl. Acad. Sci. USA *102*, 6207–6212.

Kadowaki, T., Yamauchi, T., Kubota, N., Hara, K., Ueki, K., and Tobe, K. (2006). Adiponectin and adiponectin receptors in insulin resistance, diabetes, and the metabolic syndrome. J. Clin. Invest. *116*, 1784–1792.

Kamileri, I., Karakasilioti, I., and Garinis, G.A. (2012a). Nucleotide excision repair: new tricks with old bricks. Trends Genet. *28*, 566–573.

Kamileri, I., Karakasilioti, I., Sideri, A., Kosteas, T., Tatarakis, A., Talianidis, I., and Garinis, G.A. (2012b). Defective transcription initiation causes postnatal growth failure in a mouse model of nucleotide excision repair (NER) progeria. Proc. Natl. Acad. Sci. USA *109*, 2995–3000.

Khazen, W., M'bika, J.P., Tomkiewicz, C., Benelli, C., Chany, C., Achour, A., and Forest, C. (2005). Expression of macrophage-selective markers in human and rodent adipocytes. FEBS Lett. *579*, 5631–5634.

Kim, S., Huang, L.W., Snow, K.J., Ablamunits, V., Hasham, M.G., Young, T.H., Paulk, A.C., Richardson, J.E., Affourtit, J.P., Shalom-Barak, T., et al. (2007). A mouse model of conditional lipodystrophy. Proc. Natl. Acad. Sci. USA *104*, 16627–16632.

Kimura, I., Moritani, Y., and Tanizaki, Y. (1973). Basophils in bronchial asthma with reference to reagin-type allergy. Clin. Allergy *3*, 195–202.

Li, J., Han, Y.R., Plummer, M.R., and Herrup, K. (2009). Cytoplasmic ATM in neurons modulates synaptic function. Curr. Biol. *19*, 2091–2096.

Mao, J., Yang, T., Gu, Z., Heird, W.C., Finegold, M.J., Lee, B., and Wakil, S.J. (2009). aP2-Cre-mediated inactivation of acetyl-CoA carboxylase 1 causes growth retardation and reduced lipid accumulation in adipose tissues. Proc. Natl. Acad. Sci. USA *106*, 17576–17581.

Miyake, Y., and Yamasaki, S. (2012). Sensing necrotic cells. Adv. Exp. Med. Biol. *738*, 144–152.

Murano, I., Barbatelli, G., Parisani, V., Latini, C., Muzzonigro, G., Castellucci, M., and Cinti, S. (2008). Dead adipocytes, detected as crown-like structures, are prevalent in visceral fat depots of genetically obese mice. J. Lipid Res. *49*, 1562–1568.

Niedernhofer, L.J., Daniels, J.S., Rouzer, C.A., Greene, R.E., and Marnett, L.J. (2003). Malondialdehyde, a product of lipid peroxidation, is mutagenic in human cells. J. Biol. Chem. *278*, 31426–31433.

Niedernhofer, L.J., Odijk, H., Budzowska, M., van Drunen, E., Maas, A., Theil, A.F., de Wit, J., Jaspers, N.G., Beverloo, H.B., Hoeijmakers, J.H., and Kanaar, R. (2004). The structure-specific endonuclease Ercc1-Xpf is required to resolve DNA interstrand cross-link-induced double-strand breaks. Mol. Cell. Biol. *24*, 5776–5787.

Niedernhofer, L.J., Garinis, G.A., Raams, A., Lalai, A.S., Robinson, A.R., Appeldoorn, E., Odijk, H., Oostendorp, R., Ahmad, A., van Leeuwen, W., et al. (2006). A new progeroid syndrome reveals that genotoxic stress suppresses the somatotroph axis. Nature *444*, 1038–1043.

Nishimura, S., Manabe, I., Nagasaki, M., Seo, K., Yamashita, H., Hosoya, Y., Ohsugi, M., Tobe, K., Kadowaki, T., Nagai, R., and Sugiura, S. (2008). In vivo imaging in mice reveals local cell dynamics and inflammation in obese adipose tissue. J. Clin. Invest. *118*, 710–721.

Perissi, V., Jepsen, K., Glass, C.K., and Rosenfeld, M.G. (2010). Deconstructing repression: evolving models of co-repressor action. Nat. Rev. Genet. *11*, 109–123.

Rodier, F., Coppé, J.P., Patil, C.K., Hoeijmakers, W.A., Muñoz, D.P., Raza, S.R., Freund, A., Campeau, E., Davalos, A.R., and Campisi, J. (2009). Persistent DNA damage signalling triggers senescence-associated inflammatory cytokine secretion. Nat. Cell Biol. *11*, 973–979.

Satir, P., Pedersen, L.B., and Christensen, S.T. (2010). The primary cilium at a glance. J. Cell Sci. *123*, 499–503.

Sato, K., Ishiai, M., Toda, K., Furukoshi, S., Osakabe, A., Tachiwana, H., Takizawa, Y., Kagawa, W., Kitao, H., Dohmae, N., et al. (2012). Histone chaperone activity of Fanconi anemia proteins, FANCD2 and FANCI, is required for DNA crosslink repair. EMBO J. *31*, 3524–3536.

Schumacher, B., Hoeijmakers, J.H., and Garinis, G.A. (2009). Sealing the gap between nuclear DNA damage and longevity. Mol. Cell. Endocrinol. *299*, 112–117.

Selfridge, J., Hsia, K.T., Redhead, N.J., and Melton, D.W. (2001). Correction of liver dysfunction in DNA repair-deficient mice with an ERCC1 transgene. Nucleic Acids Res. *29*, 4541–4550.

Sepe, A., Tchkonia, T., Thomou, T., Zamboni, M., and Kirkland, J.L. (2011). Aging and regional differences in fat cell progenitors - a mini-review. Gerontology *57*, 66–75.

Sims, G.P., Rowe, D.C., Rietdijk, S.T., Herbst, R., and Coyle, A.J. (2010). HMGB1 and RAGE in inflammation and cancer. Annu. Rev. Immunol. *28*, 367–388.

Straus, D.S., and Glass, C.K. (2007). Anti-inflammatory actions of PPAR ligands: new insights on cellular and molecular mechanisms. Trends Immunol. *28*, 551–558.

Tang, W., Zeve, D., Suh, J.M., Bosnakovski, D., Kyba, M., Hammer, R.E., Tallquist, M.D., and Graff, J.M. (2008). White fat progenitor cells reside in the adipose vasculature. Science *322*, 583–586.

Tchkonia, T., Morbeck, D.E., Von Zglinicki, T., Van Deursen, J., Lustgarten, J., Scrable, H., Khosla, S., Jensen, M.D., and Kirkland, J.L. (2010). Fat tissue, aging, and cellular senescence. Aging Cell *9*, 667–684.

Verhagen-Oldenampsen, J.H., Haanstra, J.R., van Strien, P.M., Valkhof, M., Touw, I.P., and von Lindern, M. (2012). Loss of ercc1 results in a time- and dose-dependent reduction of proliferating early hematopoietic progenitors. Anemia *2012*, 783068.

Weeda, G., Donker, I., de Wit, J., Morreau, H., Janssens, R., Vissers, C.J., Nigg, A., van Steeg, H., Bootsma, D., and Hoeijmakers, J.H. (1997). Disruption of mouse ERCC1 results in a novel repair syndrome with growth failure, nuclear abnormalities and senescence. Curr. Biol. *7*, 427–439.

Yang, D.Q., and Kastan, M.B. (2000). Participation of ATM in insulin signalling through phosphorylation of eIF-4E-binding protein 1. Nat. Cell Biol. *2*, 893–898.

Yang, D.Q., Halaby, M.J., Li, Y., Hibma, J.C., and Burn, P. (2011). Cytoplasmic ATM protein kinase: an emerging therapeutic target for diabetes, cancer and neuronal degeneration. Drug Discov. Today *16*, 332–338.